JOURNAL OF MATERIALS SCIENCE **38** (2003) 3797–3807

Effect of superalloy substrate composition on the performance of a thermal barrier coating system

H. M. TAWANCY, A. I. MOHAMED, N. M. ABBAS
Materials Characterization Laboratory, Center for Engineering Research, Research Institute, King Fahd University of Petroleum and Minerals, P.O. Box 1639, Dhahran 31262, Saudi Arabia
E-mail: tawancy@kfupm.edu.sa

R. E. JONES, D. S. RICKERBY
Rolls-Royce plc, Derby, UK

An investigation was carried out to determine the performance of a thermal barrier coating system consisting of (ZrO_2-8% Y_2O_3)/(Pt) on two single-crystal Ni-base superalloys. Coating/alloy behavior was studied with reference to: (i) initial microstructural features, (ii) oxidation properties, (iii) thermal stability characteristics, and (iv) failure mechanism. All thermal exposure tests were carried out at 1150°C in still air with a 24-h cycling period to room temperature. Failure of the coating system was indicated by macroscopic spallation of the ceramic top coat. Scanning electron microscopy combined with energy dispersive X-ray spectroscopy as well as X-ray diffraction were used to characterize the microstructure.

Decohesion between the thermally grown oxide and bond coat was found to be the mode of failure of the coating system for both alloys. This was correlated with the formation of Ti-rich and/or Ti+Ta-rich oxide particles near the oxide-bond coat interface degrading the adherence of the thermally grown oxide. However, the thickening rate of the oxide had very little or no effect on the relative coating performance. It was concluded that the coating performance is critically dependent on alloy substrate composition particularly the concentration of elements, which could have adverse effects on oxidation resistance such as Ti.

1. Introduction

Application of thermal barrier coatings (TBC) as surface protection systems for gas turbine blades allows the turbine entry temperature to be increased by as much as 50–100°C equivalent to 2–4 generations of superalloy development. Therefore, there has been an increasing interest in better understanding the behavior of these coatings. Typically, the coating system consists of a metallic layer of bond coat deposited on the superalloy substrate followed by a ceramic layer of top coat. Although a wide variety of bond coats is available, a layer of ZrO_2 stabilized by 8 weight% Y_2O_3 is used as the ceramic top coat. It is the primary function of the bond coat to develop a layer of Al_2O_3 scale acting as a glue holding the top coat to the underlying bond coat/superalloy substrate. Prior to exposure at elevated temperatures, the coating/alloy system is given a standard heat treatment so that the bond coat develops a layer of Al_2O_3 scale about 1 μm in thickness holding the top coat. This is differentiated from the oxide developed upon subsequent exposure at elevated temperatures, which is commonly known as thermally grown oxide.

In general, the performance of TBC systems in gas turbine blade applications is limited by the adhesion of the ceramic top coat. Earlier studies had demonstrated that the most common failure mode of TBC systems is loss of adhesion between the thermally grown oxide and underlying bond coat [1–6]. Therefore, oxide adhesion can be considered as the weakest link in the system. Since bond coats can be degraded by interdiffusion with the superalloy substrate similar to the case of conventional coatings [7], the chemical composition of the superalloy substrate is expected have a significant effect on the performance of TBC systems using a given bond coat. Although overlay bond coats were found to provide superior performance [8], the use of Pt bond coats can also provide an acceptable level of protection. Therefore, this study was undertaken to determine the effect of superalloy substrate composition on the performance of TBC systems using a layer of Pt as a bond coat.

2. Experimental procedure

Two single-crystal superalloys were included in this study and identified by their nominal compositions as

TABLE I Nominal chemical compositios of alloys 1 and 2 (weight%)

Element	Ni	Co	Cr	Al	Ti	Ta	W	Re	Mo	Hf
Alloy 1	Bal.	9.5	6.2	5.5	1.0	6.5	6.5	2.9	0.6	0.1
Alloy 2	Bal.	9.5	6.2	5.5	0.3	8.5	6.5	6.0	0.6	0.1

alloy 1 and alloy 2 in Table I. As can be seen, alloy 1 contains more Ti and less Re than alloy 2. Coated samples were prepared by deposition of about 10 μm thick layer of Pt on the alloy surface followed by a layer of the ceramic top coat (ZrO_2 + 8 weight% Y_2O_3) of 250 μm nominal thickness using the electron beam-physical vapor deposition (EB-PVD) technique. Subsequently, the bond coat microstructure was developed by a diffusion heat treatment in vacuum at 1150°C where the Pt layer is allowed to interact with the underlying alloy substrate. Comparative coating performance was determined by thermal exposure tests at 1150°C in still air with a 24-h cycling period to room temperature until failure of the coating system occurred as indicated by spallation of the ceramic top coat. Scanning electron microscopy combined with energy dispersive X-ray spectroscopy as well as X-ray diffraction were used to characterize the coating microstructure.

3. Results and discussion

3.1. Development of the microstructure of bond coat

Gross microstructural features of a cross-section the coating/alloy system in the heat-treated condition are summarized in Fig. 1. As shown in Fig. 1a, the ceramic top coat of about 230 μm thickness has a columnar grain structure. It is separated from the bond coat (about 30 μm in thickness) by a 1 μm layer of Al_2O_3 scale. It is to be noted that the original alloy surface is marked by alumina particles resulting from grit blasting prior to deposition of the Pt layer. Corresponding X-ray mapping images of O and Al are shown in Fig. 1b illustrating the 1 μm-Al_2O_3 layer separating the top coat from the bond coat.

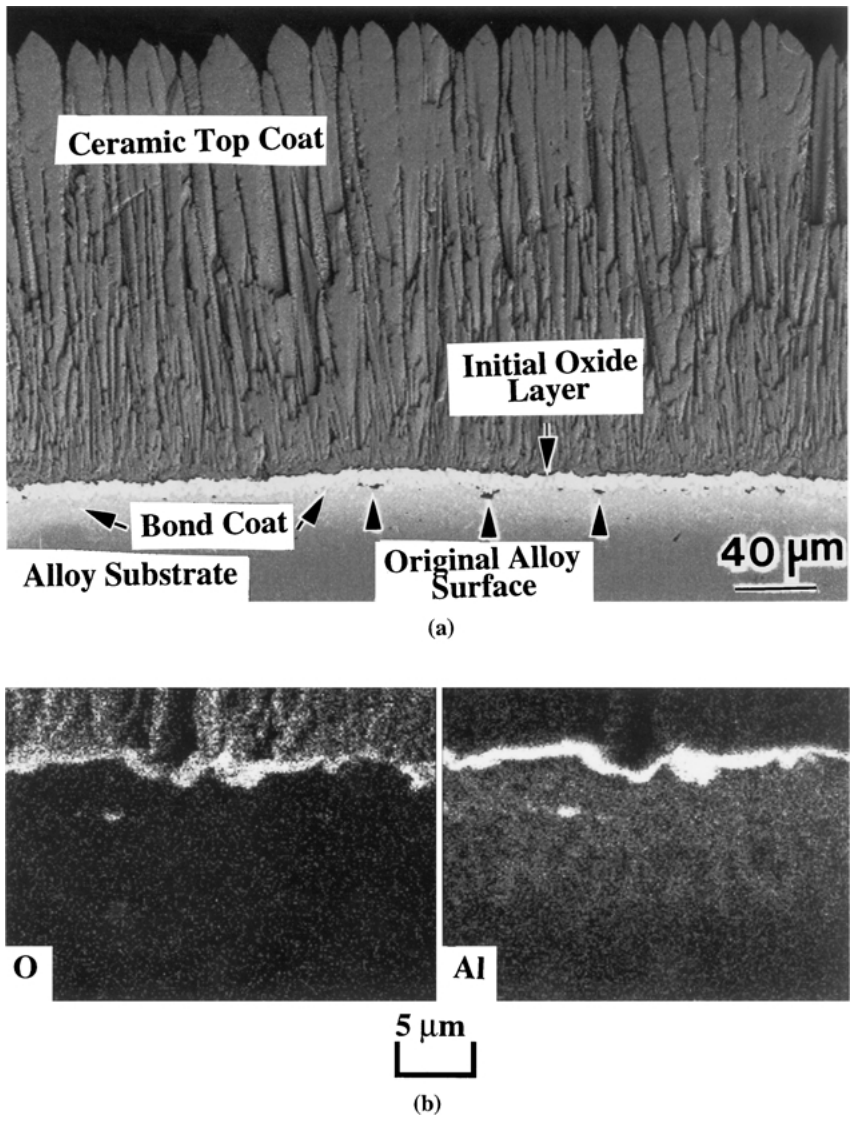

Figure 1 Characteristic microstructural features of the coating system on alloys 1 and 2 in the heat-treated condition; an example derived from alloy 1. (a) Backscattered electron image along the coating cross-section and into the alloy substrate. (b) Corresponding X-ray mapping images of O and Al illustrating the initial oxide layer between the top coat and bond coat.

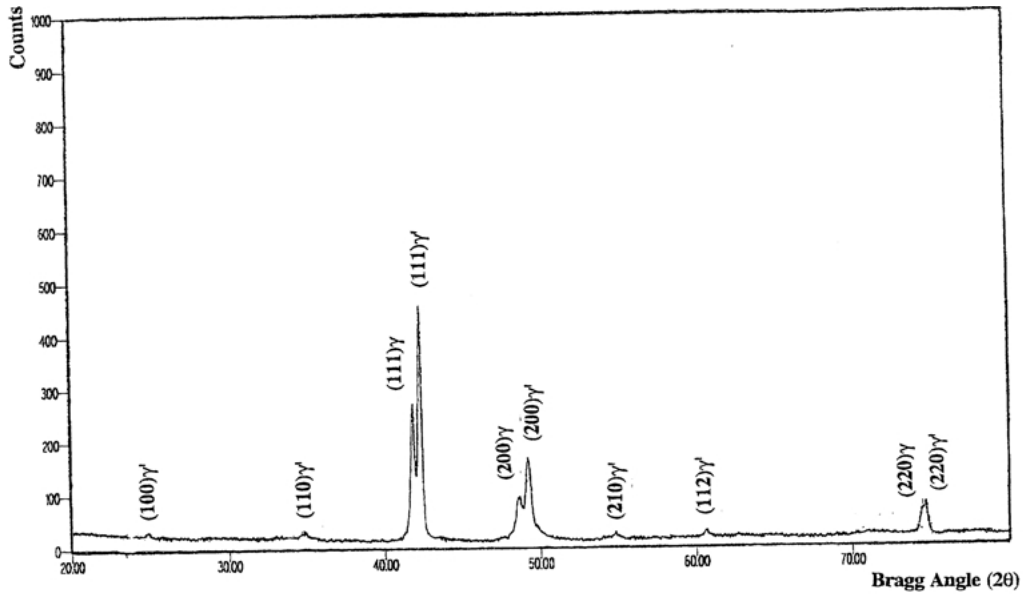

(a)

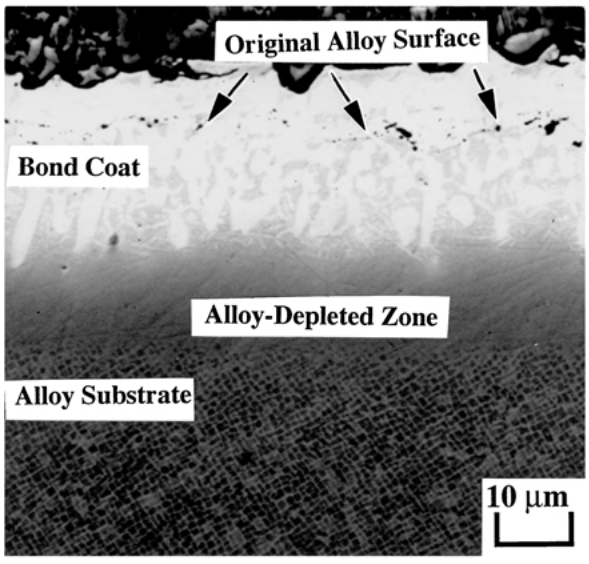

(b)

Element	Alloy 1		Alloy 2	
	γ'-Phase	γ-Phase	γ'-Phase	γ-Phase
Ni	36.25(52.45)	43.50(57.55)	36.19(55.76)	48.77(67.57)
Pt	48.19(20.98)	26.17(10.42)	51.54(23.90)	30.81(12.84)
Co	2.80(4.04)	7.07(9.31)	0.61(0.94)	2.14(2.96)
Cr	3.09(5.05)	8.30(12.40)	1.67(2.91)	4.22(6.59)
W/Re/Ta	4.26(2.00)	13.17(5.56)	5.78(2.89)	12.57(5.56)
Al	4.29(13.51)	1.46(4.22)	3.87(12.96)	1.49(4.48)
Ti	1.11(1.97)	0.33(0.53)	0.34(0.65)	-

(c)

Figure 2 Structure and composition of the bond coat on alloys 1 and 2 in the heat-treated condition. (a) A typical X-ray diffraction pattern derived from the surface layer of the bond coat (a sample free of the top coat was used in this experiment). (b) Backscattered electron image showing typical microstructural features along a cross-section of the bond coat and into the alloy substrate. (c) Typical chemical compositions of the γ'- and γ-phases near the bond coat surface for both alloys 1 and 2; weight% (atomic%).

Fig. 2 summarizes the structure and chemical compositions of the bond coats on the two alloys included in the study. X-ray diffraction patterns derived from the surface layers of the bond coat on the two alloys were identical. An example is shown in Fig. 2a. All reflections were consistently indexed in terms of γ'-phase (fcc structure, Ll_2-type superlattice), and γ-phase (fcc solid-solution). Fig. 2b illustrates a typical microstructure along a cross-section of the coating system and into the alloy substrate distinguished by the characteristic structure of γ'-phase. As further discussed later in this section, alloy substrate elements transported into the bond coat during its formation lead to the creation of an alloy-depleted zone as shown in Fig. 2b. Typical compositions of the γ'- and γ-phases near the bond coat surface for both alloys are summarized in Fig. 2c. It is observed that more Pt was partitioned into the γ'-phase contributing to its diffusional stability. Also as expected, Ta and Ti were preferentially partitioned into the γ'-phase. A one-to-one correspondence was found to exist between the Ti content of each alloy and the Ti content of the γ'-phase as can be seen by comparing the data of Fig. 2c and Table I.

Various zones constituting the bond coat were revealed at higher magnifications as demonstrated in the example of Fig. 3. It is observed that the original alloy surface (marked by residual alumina particles resulting from grit blasting) separates two sets of zones. A zone of γ-phase containing lamellar γ'-phase is observed just below the alloy surface (region marked I in

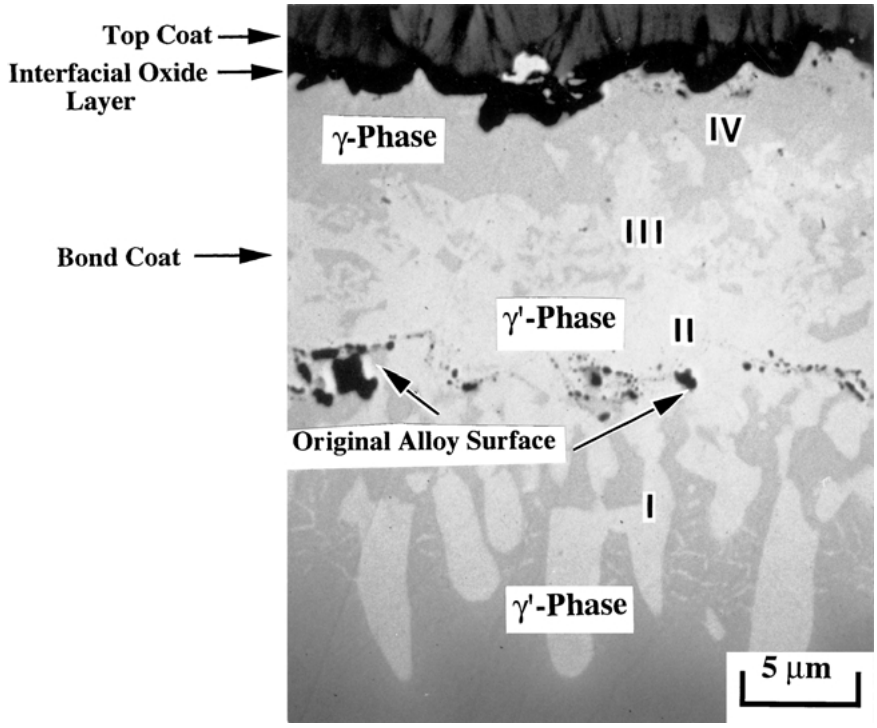

Figure 3 A backscattered electron image illustrating details of the microstructure of a cross-section of the bond coat as viewed at higher magnification; an example derived from alloy 1.

Fig. 3). Just above the alloy surface, a zone of dense and compact γ'-phase is observed (region II). This is followed by a zone consisting of a mixture of γ'- and γ-phases (region III), and then a thin surface layer consisting of predominantly γ-phase (region IV). It is to be noted that the γ'-phase present below the alloy surface was found to be enriched in transition metals particularly Ta, which could explain the characteristic lamellar morphology related to larger γ'-γ lattice mismatch.

Evolution of the bond coat microstructure shown in Fig. 3 could be explained in terms of interdiffusion between the deposited Pt layer and alloy substrate as schematically illustrated in Fig. 4. During the diffusion

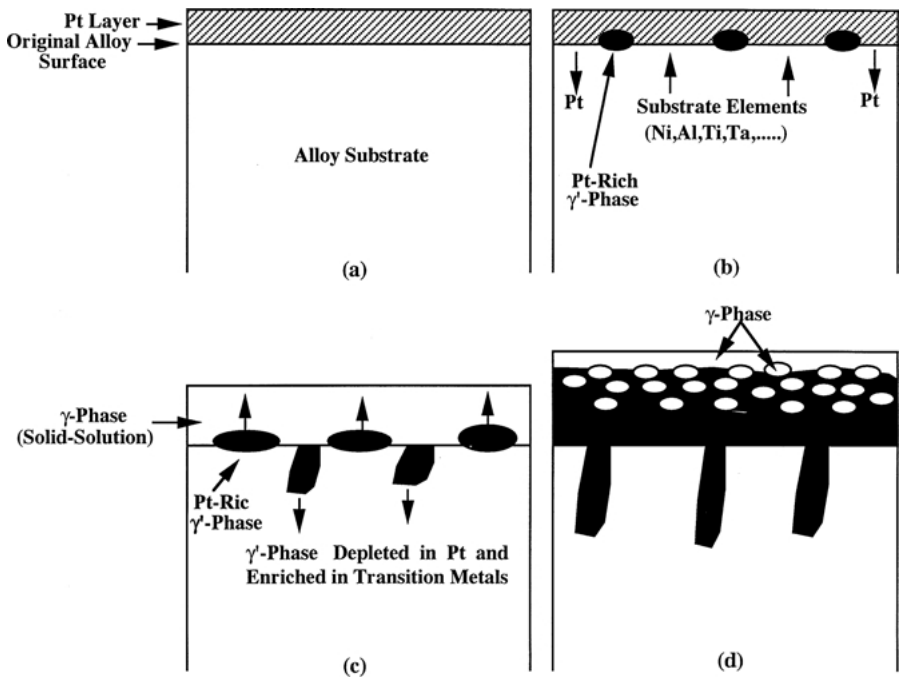

Figure 4 Schematics illustrating the evolution of the bond coat microstructure during the diffusion heat treatment. (a) Initial layer of Pt deposited on the alloy surface. (b) Nucleation of Pt-rich γ'-phase at the interface between the Pt layer and alloy substrate. (c) Outward and inward growth of the γ'-phase. (d) Final microstructure in the heat-treated condition.

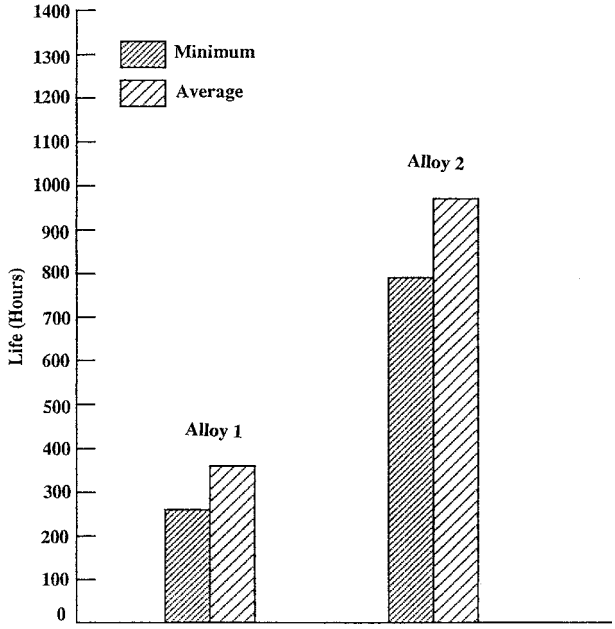

Figure 5 Comparative performance of the thermal barrier coating system on alloys 1 and 2 as derived from thermal exposure tests at 1150°C with a 24-h cycling period to room temperature.

heat treatment at 1150°C, the bond coat microstructure was developed by inward diffusion of Pt and outward diffusion of alloy substrate elements. Reaction between the Pt layer and alloy substrate is expected to be initiated at the interface resulting in the formation of a Pt-rich γ'-phase (Ll_2 superlattice). It is noted that similar to Ni, Pt can react with Al to form a γ'-phase of the type Pt_3Al. Therefore, the initial reaction at the interface could be described as:

$$3Pt(\text{deposited layer}) + Al\ (\text{alloy substrate}) \rightarrow Pt_3Al\ (\text{isomorphous with } Ni_3Al)$$

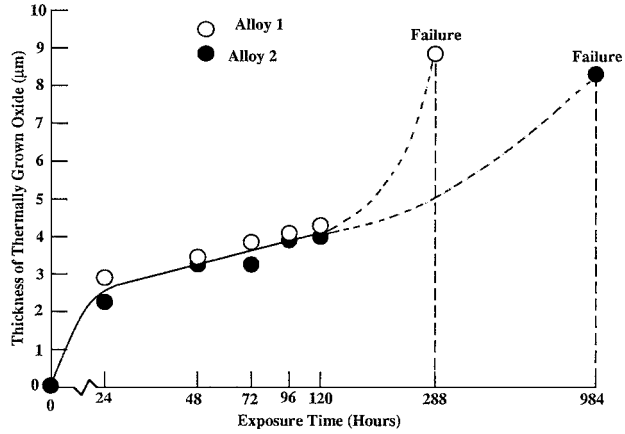

Figure 7 Comparative thickening rate of the thermally grown oxide corresponding to alloys 1 and 2 during exposure at 1150°C.

As a result of outward diffusion of Ni and other substrate elements during the later stages of heat treatment, the composition of the initially formed γ'-phase is changed particularly by the replacement of some Pt with Ni, i.e.:

$$Pt_3Al + Ni \rightarrow (Pt,Ni)_3Al$$

Further change in composition could occur by replacing some of the Ni with transition metals such as W and possibly Re as well as by replacing some of the Al by Ti and Ta. Therefore, the general composition of the γ'-phase could be of the type $(Pt,Ni,W,Re)_3(Al,Ti,Ta)$.

3.2. Comparative performance of the coating system at 1150°C

Fig. 5 shows the relative performance of the coating system on alloys 1 and 2 as determined from thermal

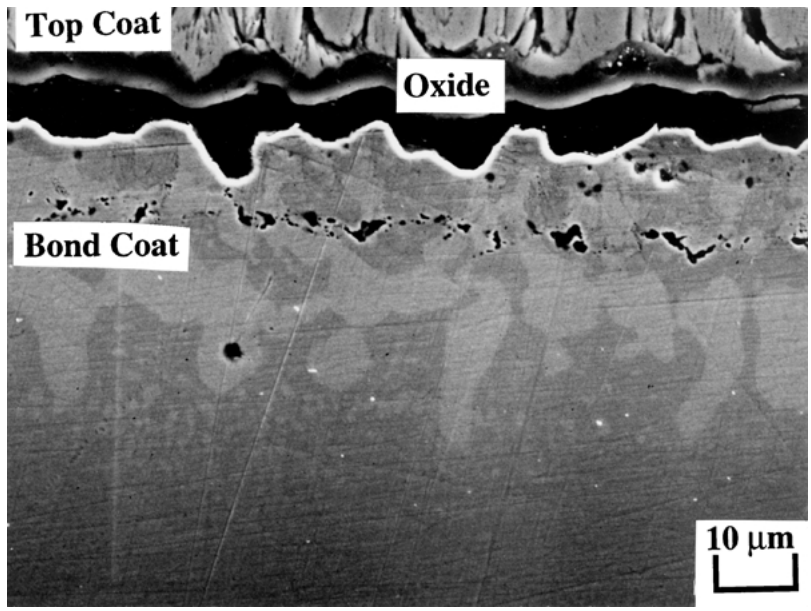

Figure 6 An example derived from alloy 1 to illustrate the typical failure mechanism of the coating system on both alloys; a secondary electron image showing localized decohesion between the bond coat and thermally grown oxide after 168 h of exposure at 1150°C.

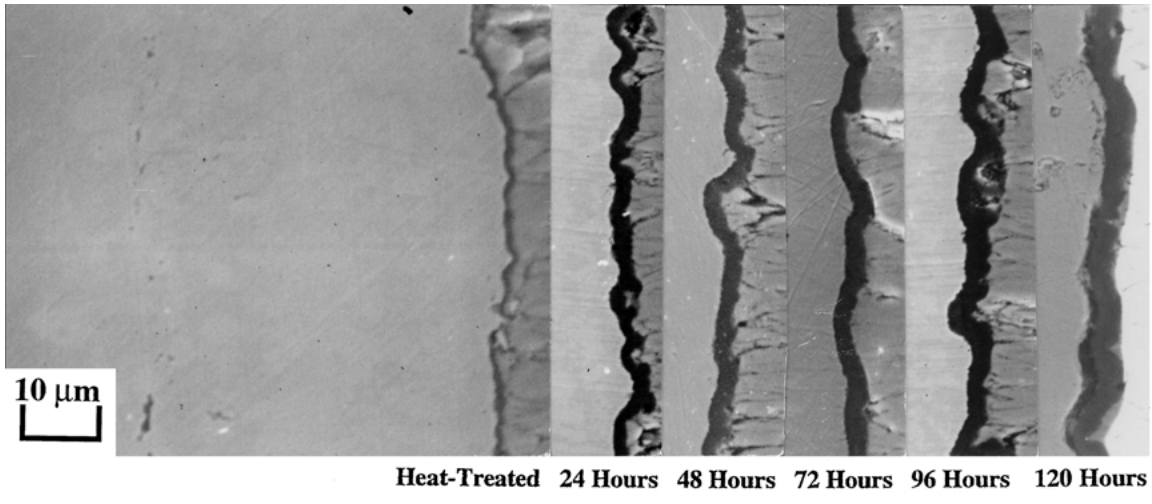

(a)

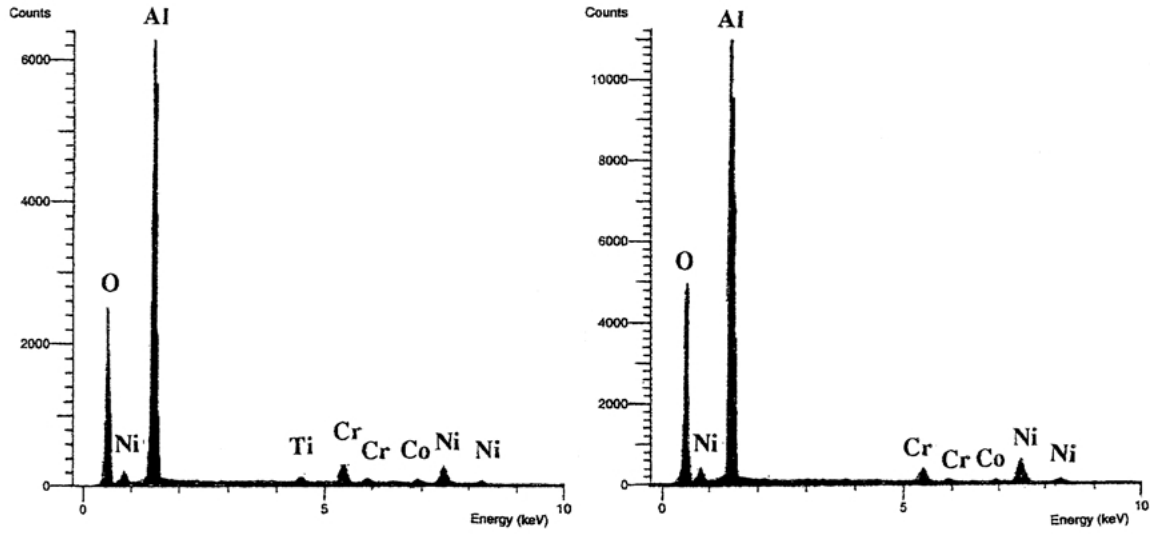

(b)

(c)

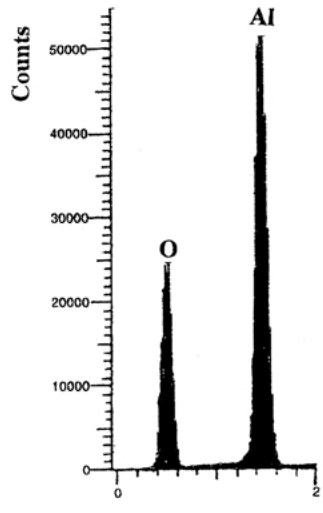

(d)

Figure 8 An example illustrating typical morphology and composition of the thermally grown oxide during exposure at 1150°C. (a) Secondary electron images derived from alloy 2 showing the effect of exposure time up to 120 h at 1150°C on the thickness of the oxide layer. (b) An energy dispersive X-ray spectrum showing typical elemental composition of the oxide corresponding to alloy 1 near the oxide-bond coat interface after. (c) An energy dispersive X-ray spectrum showing typical composition of the oxide corresponding to alloy 2 near the oxide-bond coat interface. (d) An energy dispersive X-ray spectrum illustrating typical elemental composition of the oxide near the oxide-top coat interface for both alloys 1 and 2.

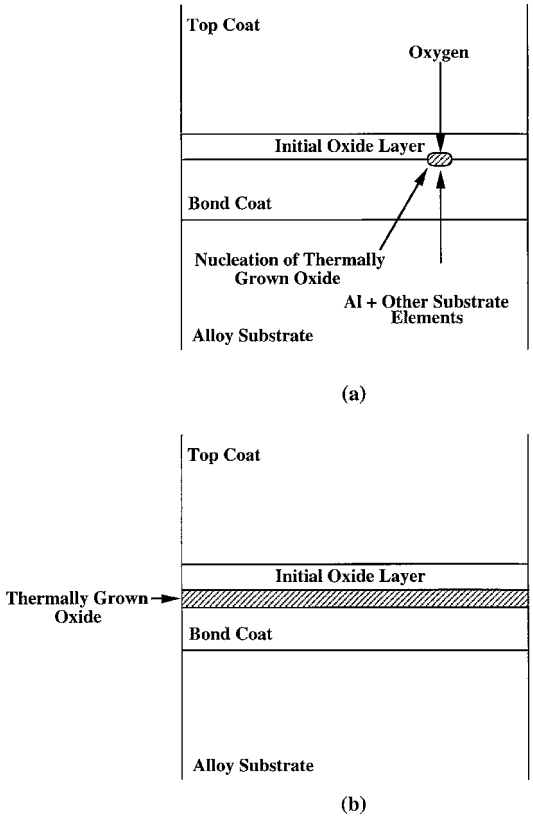

Figure 9 Schematics illustrating the growth mechanism of the thermally grown oxide. (a) Nucleation of new oxide at the initial oxide-bond coat interface by inward diffusion of oxygen. (b) Oxide growth by inward movement of the oxide-bond coat interface.

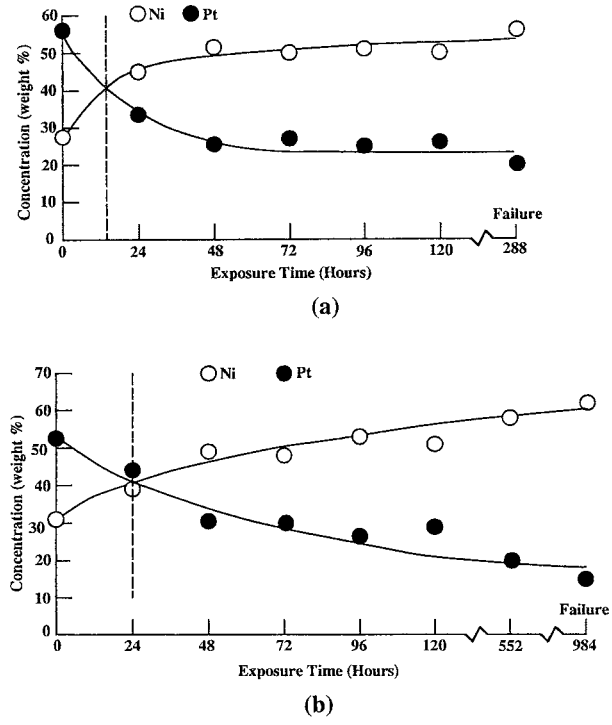

Figure 11 Effect of exposure time up to failure of the coating system at 1150°C on the Pt and Ni concentrations within the γ'-phase near the bond coat surface. (a) Alloy 1 and (b) Alloy 2.

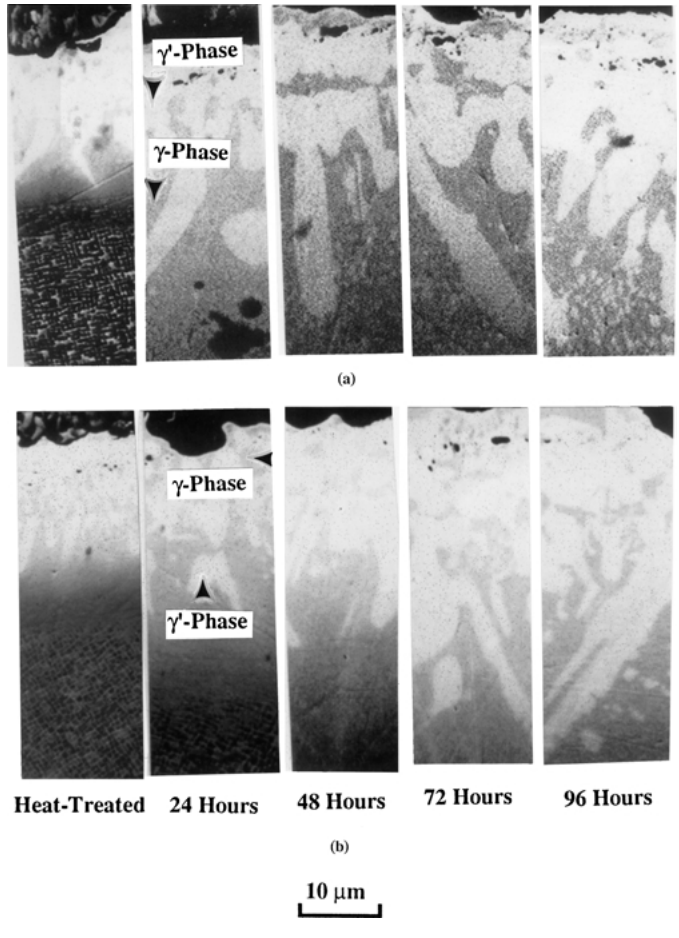

Figure 10 Backscattered electron images illustrating the effect of exposure time at 1150°C up to 120 h on the microstructure of a cross-section of the bond coat. (a) Alloy 1 and (b) Alloy 2.

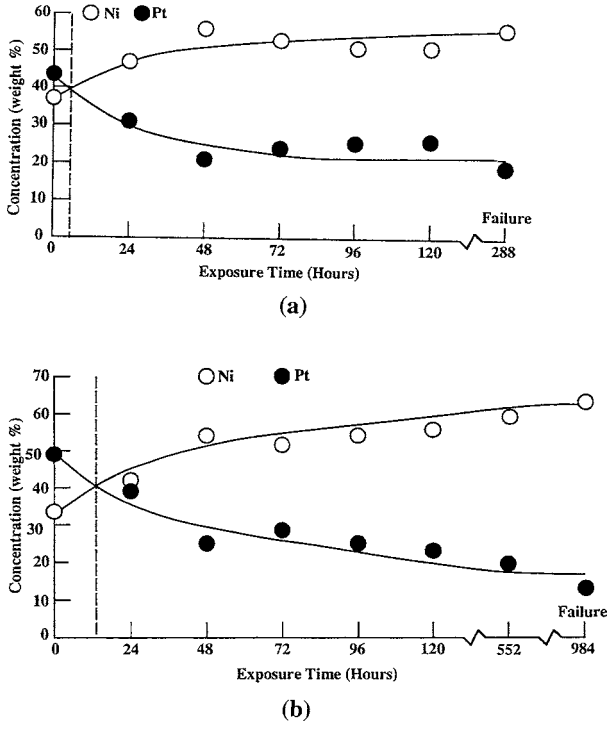

Figure 12 Effect of exposure time up to failure of the coating system at 1150°C on the Pt and Ni concentrations within the γ-phase near the bond coat surface. (a) Alloy 1 and (b) Alloy 2.

exposure tests at 1150°C with a 24-h cycling period to room temperature. It is evident that the coating on alloy 2 had a superior performance. However, for both alloys, the coating system exhibited the same failure mode involving loss of adhesion between the thermally grown oxide and bond coat as demonstrated in Fig. 6.

Comparative thickening rates of the thermally grown oxide (total oxide layer- the initial 1 μm-layer) developed by the bond coat are illustrated in Fig. 7. It is evident that the bond coat on both alloys was able to develop a protective oxide layer as indicated by the primary oxidation stage followed by a steady-state. Although the average time to failure corresponding to alloy 2 was 984 h in comparison with 288 h for alloy 1, both alloys exhibited about the same oxide thickness at the time of failure as shown in Fig. 7. This observation suggested that stresses associated with oxide growth rate had very little or no effect on the decohesion between the oxide and bond coat.

As an example, the secondary electron images of Fig. 8a show the effect of exposure time up to 120 h at 1150°C on the total oxide thickness corresponding to alloy 1. Similar results were obtained for alloy 2 as shown in the data of Fig. 7. However, near the

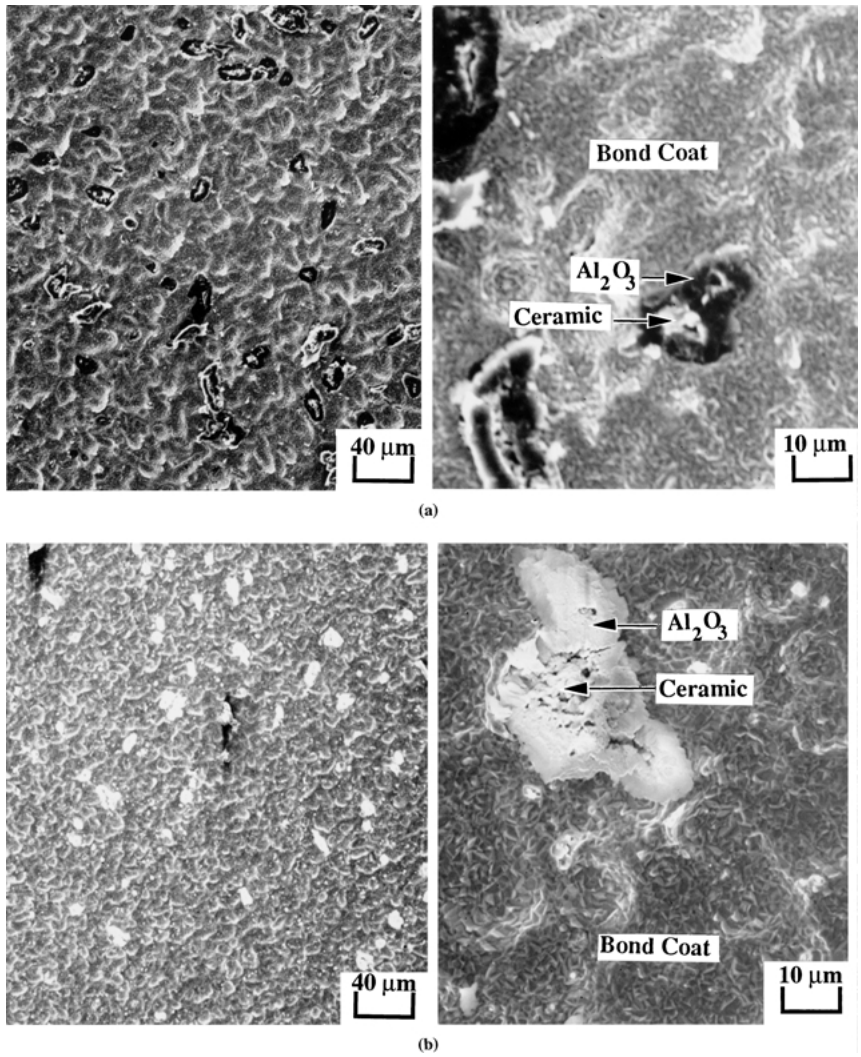

Figure 13 Secondary electron images illustrating characteristic morphological features of the bond coat surface exposed by failure during exposure at 1150°C; same area viewed at different magnifications. (a) Alloy 1 (288 h of exposure). (b) Alloy 2 (984 h of exposure).

bond coat surface, the oxide corresponding to alloy 1 (Fig. 8b) contained a small concentration of Ti in addition to other substrate elements in contrast with the case of alloy 2 where the oxide was relatively free of Ti (Fig. 8c). As shown in the example of Fig. 8d, the oxide near the bond coat-top coat interface was essentially free of substrate elements indicating that for both alloys, the thermally grown oxide was developed by inward diffusion of oxygen as schematically illustrated in Fig. 9. A similar result was reported for other coating/alloy systems [5, 9].

3.3. Thermal stability characteristics of the bond coat

Backscattered electron images illustrating the effect of exposure time up to 120 h at 1150°C on the microstructure of a cross-section of the bond coat on both alloys are shown in Fig. 10. As can be seen, both alloys exhibited a similar behavior in that a substantial coarsening of the γ'-phase occurred with continued thermal exposure. This was found to be associated with inward diffusion of Pt and outward diffusion of alloy substrate elements as demonstrated in the examples of Figs 11 and 12. It is observed that the Pt content of both the γ'- and γ-phases near the bond coat surface was decreased with continued exposure, however, most of this decrease occurred within the first 24 h of exposure. Simultaneously, there was a corresponding increase in the Ni content. Since Pt is known to promote selective oxidation of Al improving the performance of the coating system [10], the oxidation properties of the bond coat could be degraded by interdiffusion as demonstrated below.

3.4. Failure mechanism of the coating system

As indicated earlier, the failure mode of the coating system on both alloys was loss of adhesion between the thermally grown oxide and bond coat leading to spallation of the ceramic top coat. Typical morphological features of the bond coat surface exposed by failure of the coating system on both alloys are shown in the secondary electron images of Fig. 13. For both alloys, the bond coat surface exhibited similar morphological features. Islands containing Al_2O_3 scale and debris of the ceramic top coat were observed at the surface. Also, for both alloys, the surface layer of the bond coat consisted of γ-phase.

Fig. 14 shows the corresponding morphological features of the exposed surface of the top coat, which was found to be predominantly covered by Al_2O_3 scale. When viewed at higher magnifications, both surfaces

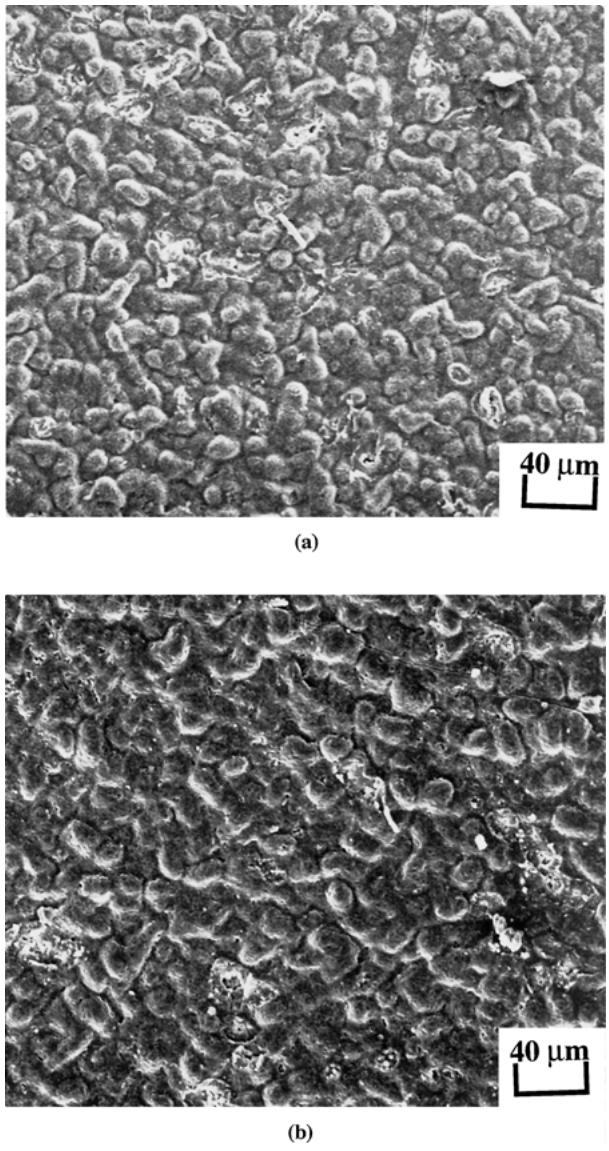

Figure 14 Secondary electron images illustrating characteristic morphological features of the surface of top coat exposed by failure during exposure at 1150°C. (a) Alloy 1 (288 h of exposure) and (b) Alloy 2 (984 h of exposure).

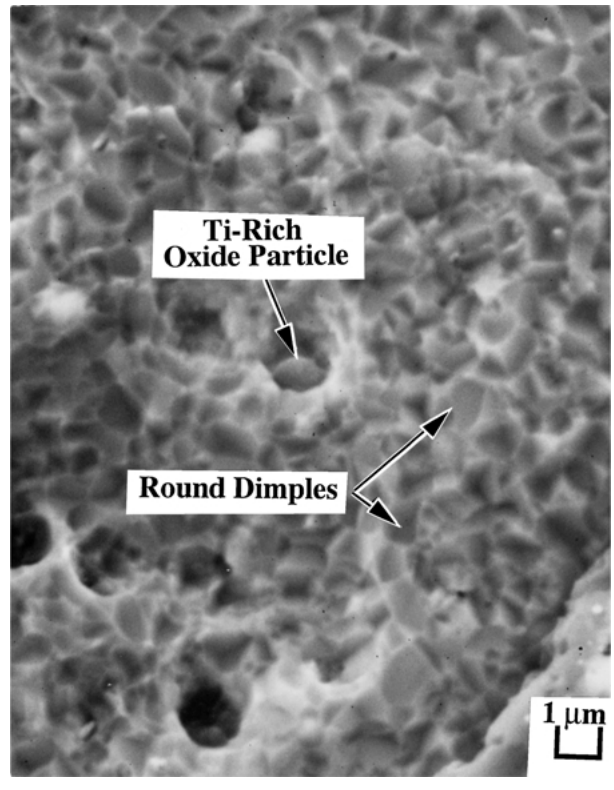

Figure 15 A secondary electron image of the bond coat surface corresponding to alloy 1 (failure after 288 h at 1150°C) showing voids containing particles of a Ti-rich oxide.

exposed by failure were found to exhibit characteristics similar to those associated with a dimple-type rupture. For example, Fig. 15 shows the morphology of the bond coat surface exposed by failure of the coating system on alloy 1 after 288 h of exposure at 1150°C. Round voids can be distinguished and occasionally, these were found to contain Ti-rich oxide particles. Some of the oxide particles were also enriched in Ta. Another example derived from the exposed surface of the top coat in the case of alloy 2 is shown in Fig. 16. Round voids within the oxide layer were also found to contain Ti+Ta-rich oxide particles

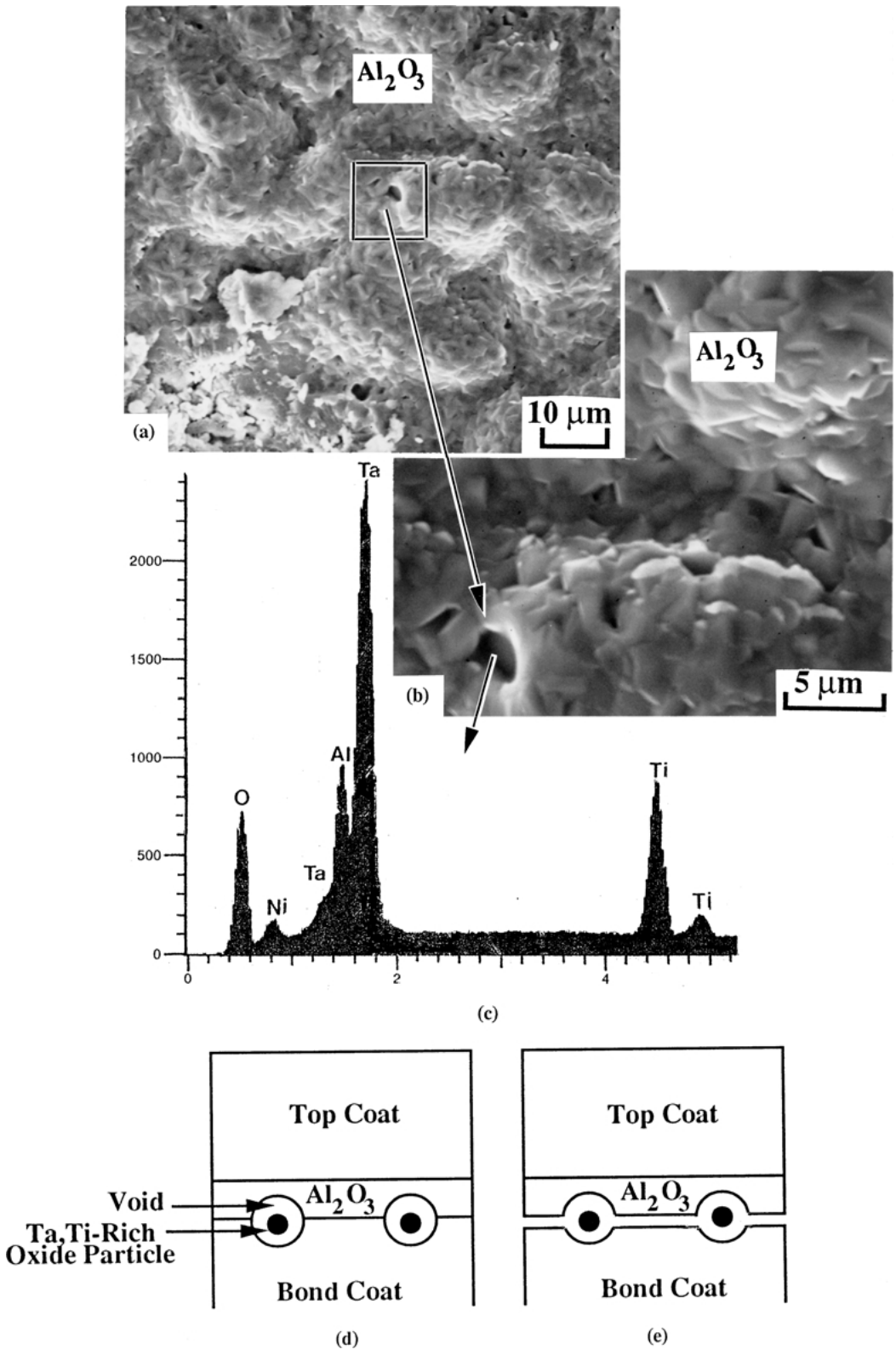

Figure 16 Identification of Ta+Ti-rich oxide at the bond coat surface corresponding to alloy 2 after failure at 1150°C (984 h of exposure). (a) and (b) are secondary electron images of the same area viewed at different magnifications. (c) Energy dispersive X-ray spectrum illustrating the elemental composition of the particle within the void in (a) and (b). (d) A schematic illustrating the formation of voids around the Ta+Ti-rich oxide particles near the oxide-bond coat interface. (e) A schematic illustrating the decoheation of the oxide by coalescence of voids around the Ta+Ti-rich oxide particles.

as illustrated in Fig. 16a and b. It is to be noted that the surface shown in Fig. 16a represents the interface between the thermally grown oxide and bond coat at the time of failure. It is evident from the results of this study that the coating system on both alloys had failed by the same mechanism, however, the process leading to failure was relatively accelerated in the case of alloy 1, which could be related to its composition as follows.

It is well known that particles of TiO_2 could degrade the adhesion of Al_2O_3 scale, e.g., see reference [11]. Therefore, it could be concluded from the above observations that the loss of adhesion between the thermally grown oxide and bond coat occurred by forming Ti-rich oxide particles near the interface as schematically shown in Fig. 16. Associated stress concentration could be relieved by forming voids around those particles. The observed round voids indicated that this process involved very little or no plastic deformation. Eventual coalescence of these voids could lead to separation between the oxide and bond coat (Fig. 16e) and in turn, spallation of the top coat. Evidently, the higher Ti content of alloy 1 (Table I) could accelerate failure by the above mechanism relative to the case of alloy 2.

4. Conclusion

It could be concluded from the results of this study that for a given type of bond coat, the growth rate of the thermally grown oxide has very little or no effect on coating performance. However, the coating life was found to be a sensitive function of superalloy substrate composition. In particular, differences in the concentration of elements known to degrade the adherence of Al_2O_3 scale such as Ti could have a significant effect on coating life.

Acknowledgments

It is a pleasure to acknowledge the financial support of Rolls-Royce plc who also provided the samples used in this study. The support of the Research Institute of King Fahd University of Petroleum is appreciated.

References

1. H. M. TAWANCY, N. SRIDHAR, N. M. ABBAS and D. S. RICKERBY, *J. Mater. Sci.* **33** (1998) 681.
2. U. DIETL, *Surf. and Coat. Tech.* **68/69** (1994) 17.
3. J. H. SUN, E. CHANG, C. H. CHAO and M. CHENG, *Oxid. Met.* **40**(5/6) (1993) 465.
4. S. M. MEIER, D. M. NISSLEY, K. D. SHEFFLER and T. A. CRUSE, *Trans. ASME* **114** (1992) 258.
5. W. LIH, E. CHANG, B. C. WU and C. H. CHAO, *Oxid. Met.* **36**(3/4) (1991) 221.
6. R. M. MILLER, *J. Eng. for Gas Turbines and Power* **111** (1989) 301.
7. H. M. TAWANCY, N. M. ABBAS and T. N. RHYS-JONES, *Surf. and Coat. Tech.* **54/55** (1992) 1.
8. H. M. TAWANCY, N. SRIDHAR, N. M. ABBAS and D. S. RICKERBY, *J. Mater. Sci.* **35** (2000) 3615.
9. U. SCHULZ, M. MENZEBACH, C. LEYENS and Y. Q. YOUNG, *Surf. and Coat. Tech.* **146/147** (2001) 117.
10. H. M. TAWANCY, N. SRIDHAR, N. M. ABBAS and D. S. RICKERBY, *J. Mater. Sci.* **35** (2000) 3615.
11. J. L. SMIALEK and G. H. MEIER, in "Superalloys II" edited by C. T. Sims, N. S. Stoloff and W. C. Hagel (Wilely-Interscience, New York, New York, 1987) p. 293.

Received 20 September 2002
and accepted 19 June 2003